remote sensing

MDPI

Letter

Seasonal Variability of SST Fronts in the Inner Sea of Chiloé and Its Adjacent Coastal Ocean, Northern Patagonia

Gonzalo S. Saldías [1,2,*], Wilber Hernández [3], Carlos Lara [4,5], Richard Muñoz [1], Cristian Rojas [3], Sebastián Vásquez [6], Iván Pérez-Santos [7,8] and Luis Soto-Mardones [1]

1 Departamento de Física, Facultad de Ciencias, Universidad del Bío-Bío, Concepción 4051381, Chile; richmunoz@udec.cl (R.M.); lsoto@ubiobio.cl (L.S.-M.)
2 Centro FONDAP de Investigación en Dinámica de Ecosistemas Marinos de Altas Latitudes (IDEAL), Valdivia 5090000, Chile
3 Programa de Magíster en Ciencias Físicas, Facultad de Ciencias, Universidad del Bío-Bío, Concepción 4051381, Chile; wilber.hernandez1701@alumnos.ubiobio.cl (W.H.); cristian.rojas2001@alumnos.ubiobio.cl (C.R.)
4 Departamento de Ecología, Facultad de Ciencias, Universidad Católica de la Santísima Concepción, Concepción 4090541, Chile; carlos.lara@ucsc.cl
5 Centro de Investigación en Recursos Naturales y Sustentabilidad (CIRENYS), Universidad Bernardo O'Higgins, Santiago 8370993, Chile
6 Instituto de Investigación Pesquera, Talcahuano 4260000, Chile; svasquez@inpesca.cl
7 Centro i-mar, Universidad de los Lagos, Puerto Mont 5480000, Chile; ivan.perez@ulagos.cl
8 Centro de Investigación Oceanográfica COPAS Sur-Austral, Concepción 4030000, Chile
* Correspondence: gsaldias@ubiobio.cl

Abstract: Surface oceanic fronts are regions characterized by high biological activity. Here, Sea Surface Temperature (SST) fronts are analyzed for the period 2003–2019 using the Multi-scale Ultra-high Resolution (MUR) SST product in northern Patagonia, a coastal region with high environmental variability through river discharges and coastal upwelling events. SST gradient magnitudes were maximum off Chiloé Island in summer and fall, coherent with the highest frontal probability in the coastal oceanic area, which would correspond to the formation of a coastal upwelling front in the meridional direction. Increased gradient magnitudes in the Inner Sea of Chiloé (ISC) were found primarily in spring and summer. The frontal probability analysis revealed the highest occurrences were confined to the northern area (north of Desertores Islands) and around the southern border of Boca del Guafo. An Empirical Orthogonal Function analysis was performed to clarify the dominant modes of variability in SST gradient magnitudes. The meridional coastal fronts explained the dominant mode (78% of the variance) off Chiloé Island, which dominates in summer, whereas the SST fronts inside the ISC (second mode; 15.8%) were found to dominate in spring and early summer (October–January). Future efforts are suggested focusing on high frontal probability areas to study the vertical structure and variability of the coastal fronts in the ISC and its adjacent coastal ocean.

Keywords: MUR SST; SST fronts; Inner Sea of Chiloé; northern Patagonia

Citation: Saldías, G.S.; Hernandez, W.; Lara, C.; Muñoz, R.; Rojas, C.; Vásquez, S.; Pérez-Santos, I.; Soto-Mardones, L. Seasonal Variability of SST Fronts in the Inner Sea of Chiloé and Its Adjacent Coastal Ocean, Northern Patagonia. *Remote Sens.* **2021**, *13*, 181. https://doi.org/10.3390/rs13020181

Received: 30 November 2020
Accepted: 4 January 2021
Published: 7 January 2021

1. Introduction

Oceanic fronts are relatively narrow regions with high gradients of physical, chemical, biological, and optical properties. They are generally associated with convergence at the surface [1] and high aggregation of organisms and biological activity e.g., [2,3]. Lately, enhanced submesoscale activity has been identified around fronts [4,5], which involves ageostrophic vertical circulation with increased vertical fluxes of tracers and momentum. In general, frontal features and currents such as jets and meanders e.g., [6,7], filaments e.g., [8,9], and river discharges e.g., [10,11] present distinct patterns of variation in strength and duration over multiple temporal scales and are identified from satellite sea surface temperature (SST) fields.

Remotely sensed data have been crucial in the study of the evolution of ocean fronts at multiple spatio-temporal scales [9,12–16]. The improved accuracy and spatial resolution of SST sensors over time have allowed the quantification and spatial distribution of sharp fronts in coastal regions [11,15,17–20]. Here, high-resolution (1 km) SST images are used to analyze the variability of SST fronts in the Inner Sea of Chiloé (ISC) and adjacent coastal ocean (northern Chilean Patagonia). The ISC is a long inner sea (about 260 km) with high heterogeneity of hydrographic conditions due to the influence of freshwater from several rivers and the marine influence by the active water exchange through Boca del Guafo and Chacao channel [21,22]. Several islands (Desertores Islands) promote contrasting hydrographic and SST characteristics between the northern and southern areas. In general, northern Patagonia is characterized by elevated surface chlorophyll-a concentration and primary productivity during spring-summer-fall [23]. Recently, harmful algal blooms events were described in the region in association with anomalous oceanographic conditions during summer 2016 [24]. Although the development of chlorophyll patches and blooms have been suggested to develop around frontal regions [25], there are no major insights into the evolution and distribution of surface fronts along the ISC.

This study aims to characterize the seasonal and interannual variability of surface thermal fronts along the Inner Sea of Chiloé and its adjacent coastal ocean. For the first time, high-resolution satellite images were used to achieve a frontal analysis of this region. Section 2 describes the data and methods. Section 3 resumes the principal results and discusses the seasonal and interannual evolution of SST fronts. Finally, a summary is presented in Section 4.

2. Satellite Data and Methods

We used daily SST data from the Multi-scale Ultra-high Resolution (MUR) product [18] obtained from the Physical Oceanography Distributed Active Archive Center (PODAAC; see Data Availability Statement below). MUR data were chosen over other SST products due to the increased data cover and improved performance detecting SST gradients in the coastal region [18]. The data have a spatial resolution of 0.01 × 0.01 degrees. A comparison with a near-surface temperature time series from a buoy located in Seno Reloncaví (see Figure 1) validates the performance of MUR SST in the ISC (Figure 1b,c). The buoy has been maintained by the research center i-mar since 2017 (see Data Availability Statement below).

The gradient magnitude (GM) and the Canny edge-detection algorithm [26] were used to detect and quantify the frontal regions and their evolution. The GM was computed following other studies e.g., [11,18]:

$$\nabla_x TSM_i = (TSM_{i-1} - TSM_{i+1})/(X_{i-1} - X_{i+1}) \tag{1}$$

$$\nabla_y TSM_j = (TSM_{j-1} - TSM_{j+1})/(Y_{j-1} - Y_{j+1}) \tag{2}$$

$$\mid \nabla TSM \mid = \{(\nabla_x TSM_i)^2 + (\nabla_y TSM_j)^2\}^{1/2} \tag{3}$$

where $\bigtriangledown_x SST_i$ and $\bigtriangledown_y SST_j$ are the zonal and meridional components of the SST gradient, respectively, and $| \bigtriangledown SST|$ is the gradient magnitude. The Canny edge-detection algorithm [26] was applied on daily SST fields to identify coherent frontal segments and compare them with the regions of increased gradient magnitudes. The Canny method tracks the direction of SST gradients using a threshold value. The gradients are calculated using the derivative of a Gaussian filter. After studying the range of gradient magnitudes for all images (Figure 1d), we used a high threshold value of 0.1 °C/km, which separates most values in the low range of the PDF from the higher values associated with the formation of SST fronts. The probability of finding a front was calculated as the number of times a pixel is classified as a front divided by the total images considered in a time window (i.e., seasonal aggregates). Further details of the application of the Canny method can be found elsewhere [15,19].

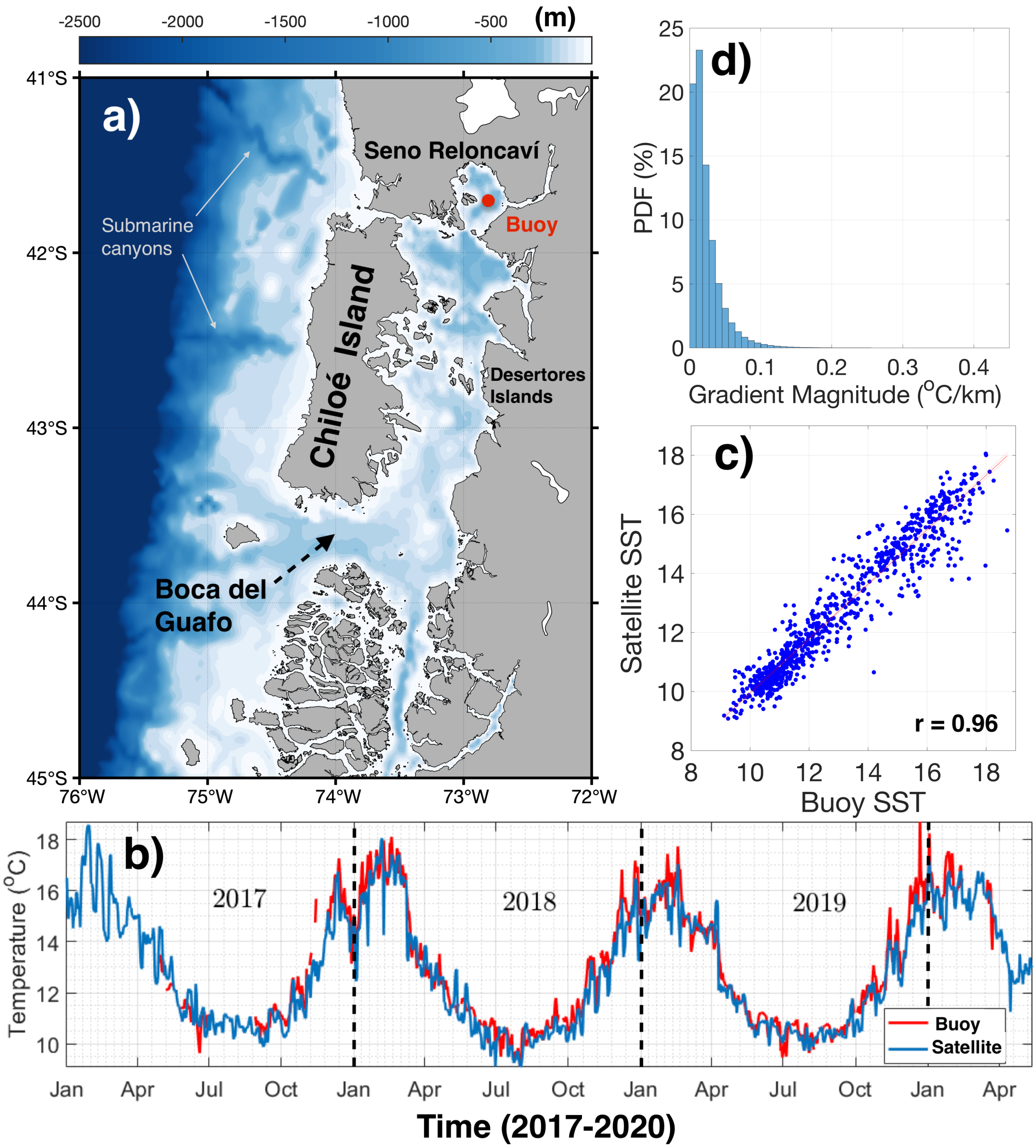

Figure 1. (**a**) Map of the Inner Sea of Chiloé and its adjacent coastal ocean in northern Patagonia. The bathymetry is shown in a blue-white color scale. The position of the oceanographic buoy located in Seno Reloncaví is denoted by a red dot. The comparison between satellite SST and near-surface (1 m) temperature at the buoy is presented in (**b**,**c**). In situ temperature has been daily averaged to match satellite SST data. (**d**) Probability Density Function (in %) of the distribution of all SST gradient magnitudes for the period 2003–2019.

Satellite chlorophyll fluorescence (Fluorescence Line Height, nFLH) data from the Moderate Resolution Imaging Spectroradiometer (MODIS, on-board Aqua) and for the period 2003–2019 were obtained from the ocean color website (see Data Availability Statement below). These data were used to compute the seasonal climatology. We chose to use the chlorophyll fluorescence over the chlorophyll product because of the characteristic estuarine turbid conditions of the ISC and the relatively poor performance of default chlorophyll algorithms [27].

An Empirical Orthogonal Function (EOF) analysis was performed on the gradient magnitudes to separate the main modes of variability. The EOF was computed following the Singular Value Decomposition (SVD) approach to avoid a large covariance matrix associated with the high resolution of the images [28]. Please note that each time series is demeaned and detrended in the process.

3. Results and Discussion

The temporal pattern of SST variability is well-captured by MUR SST compared to the buoy measurements at Seno Reloncaví for the period 2017–2020, as shown in Figure 1b. However, some events with peaks in *in situ* temperature were not well recorded by the satellite data, especially during spring-summer (Figure 1b). There is a slight underestimation by MUR SST (Figure 1c). In general, MUR data reproduced the temporal SST variability with high correlation (r = 0.96), which gave us confidence that the MUR product is reasonably accurate in these coastal waters. Given the recent deployment of this buoy in Seno Reloncaví (starting in 2017), this is the first comparison of satellite SST and *in situ* temperature in the ISC.

The seasonal climatology of SST fields revealed a typical pattern for temperate ecosystems, i.e., marked spatial and seasonal variability. During austral spring and summer, the higher SST is observed in the northern area (north of Desertores Islands) and adjacent coastal ocean (Figure 2a,d). In fall, The adjacent coastal ocean showed the highest values compared to the ISC (Figure 2b), whereas the entire coastal ocean shows the lowest temperatures (<11 °C) in winter (Figure 2c). The persistence of these mean fields is variable depending on the location and season (Figure 2e–h). The mean warm pattern observed in summer in the northern ISC (Seno Reloncaví) is also highly variable (Figure 2e). This strong variability is also presented in the fall and spring (Figure 2f,h). In general, the ICS presents the largest SST variability (greater than 1.2 °C) in spring (Figure 2h). Notice that low variability south of Desertores Islands is associated with the lowest averaged SST fields in connection with the coastal ocean through Boca del Guafo (Figure 2b,d), characterized by intrusions of Sub-Antarctic waters (SAAW) [29,30]. Finally, winter represents the coldest season with the annual cycle's greatest spatial homogeneity (Figure 2c,g). The annual cycle of SST is coherent with previous studies in northern Patagonia [22,31,32].

The quantification of the climatological SST gradient magnitudes for the entire 17 years of study is shown in Figure 3. During spring and summer, the SST gradient magnitude fields suggest a high frontal activity in the northern area of the ISC (Figure 3a,d). Summer also represents a period with increased SST fronts in the coastal ocean with an extended meridional band of high gradients (Figure 3a). This would be linked with the development of a coastal upwelling front off Chiloé Island in summer due to predominant northward winds [30,33]. The extended band with medium values of gradient magnitude in fall would represent the weakening of upwelling-favorable winds, and consequently, a weaker upwelling front (Figure 3b). Medium values in the standard deviation corresponding to the upwelling front would explain a synoptic variability with pulses of upwelling events through summer and fall (Figure 3e,f). High values in SST gradient (>0.05 °C/km) and variability (>0.03 °C/km) on the southern area of the ISC in summer could be associated with the generation of SST fronts from the intrusions of oceanic waters through Boca del Guafo (~44°S) (Figure 3a,e). In spring, the highest gradients are presented in the northern ISC with a band of increased variability near Desertores Islands (Figure 3d,h). Finally, SST's gradient magnitudes are less pronounced in winter (Figure 3c,g) which is coherent with a more homogeneous and cold temperature field (Figure 2c,g). Water column stratitication in Seno Reloncaví (not shown) presents a coherent annual cycle with maximum (minimum) stratification in spring-summer (fall-winter).

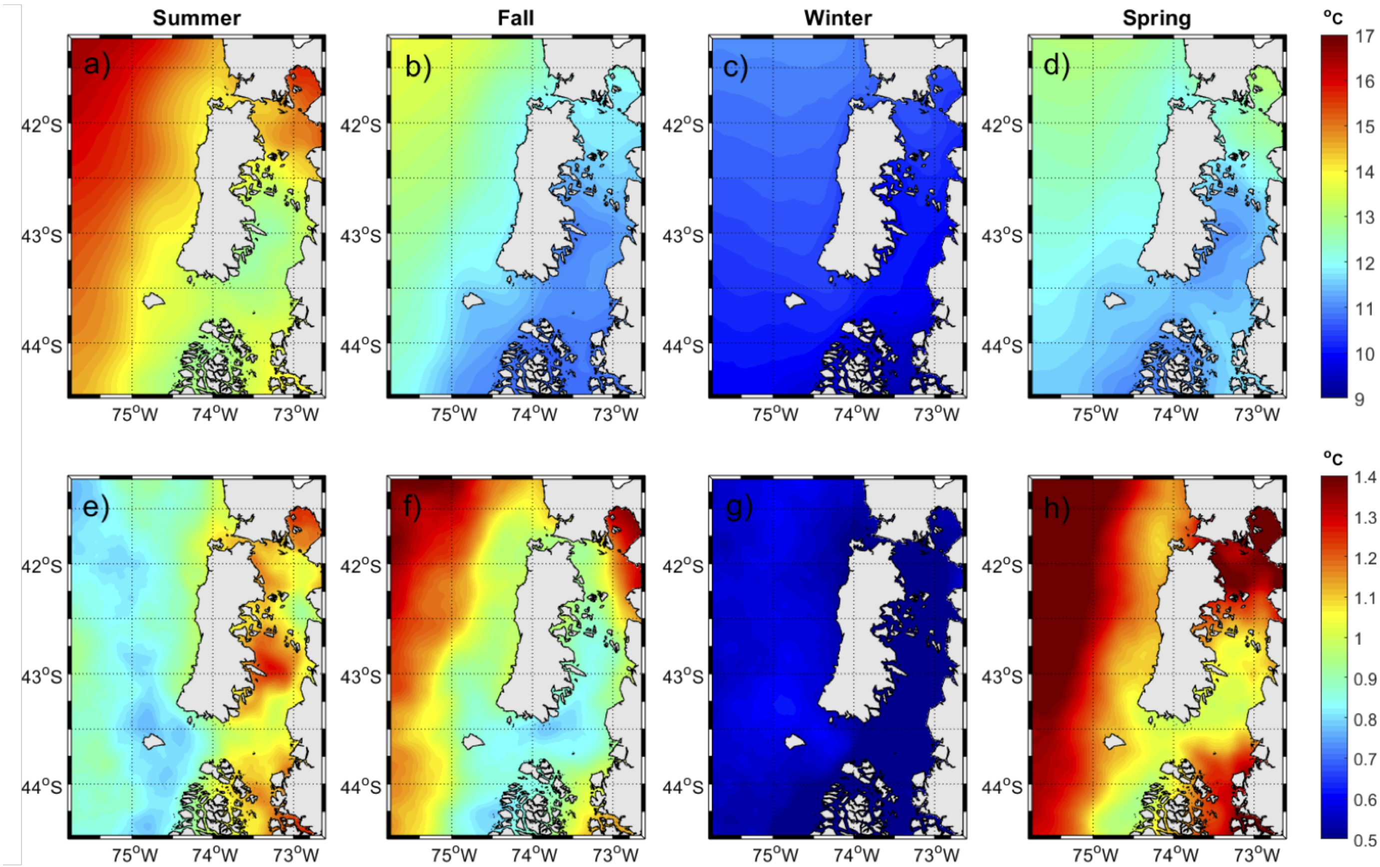

Figure 2. Seasonal climatology (2003–2019) of SST in the Inner Sea of Chiloé and its adjacent coastal ocean. (upper panels) averages and (lower panels) standard deviations for (**a**,**e**) summer (January, February, March), (**b**,**f**) fall (April, May, June), (**c**,**g**) winter (July, August, September), and (**d**,**h**) spring (October, November, December). For reference of locations see Figure 1a.

To further understand the generation and evolution of fronts along the ISC and its adjacent coastal ocean, the seasonal variability of frontal probability (FP) is shown in Figure 4. The use of an edge-detection algorithm is crucial for calculating the FP since fronts tend to be narrow and coherent bands of increased gradients of ocean properties [14], which can be overlooked and or not correctly identified through the gradient magnitude. The FP maps reveal that the formation of SST fronts off Chiloé Island in summer-fall (Figure 4a,b), potentially associated with the coastal upwelling, is consistent with the increased gradient magnitudes shown in Figure 3. The FP reaches its largest values (>9%) in the northern ISC in spring-summer (Figure 4a,d). Also, the lowest SST frontal activity in spring-summer is shown on the western section of the southern ISC (Figure 4a,d), which might be associated with a greater oceanic influence on the eastern side. The eastern side also has several river outflows, which could influence the temperature field, creating increased gradients. It is interesting to note that the FP in fall is <3% along most of the ISC, representing the season with the lowest SST frontal activity (Figure 4b). In contrast, the frontal probability values during winter indicate higher PF as compared to fall (Figure 4c vs. Figure 4b), especially at Boca del Guafo (values up to 7%), which was not demonstrated through the gradient magnitude (Figure 3).

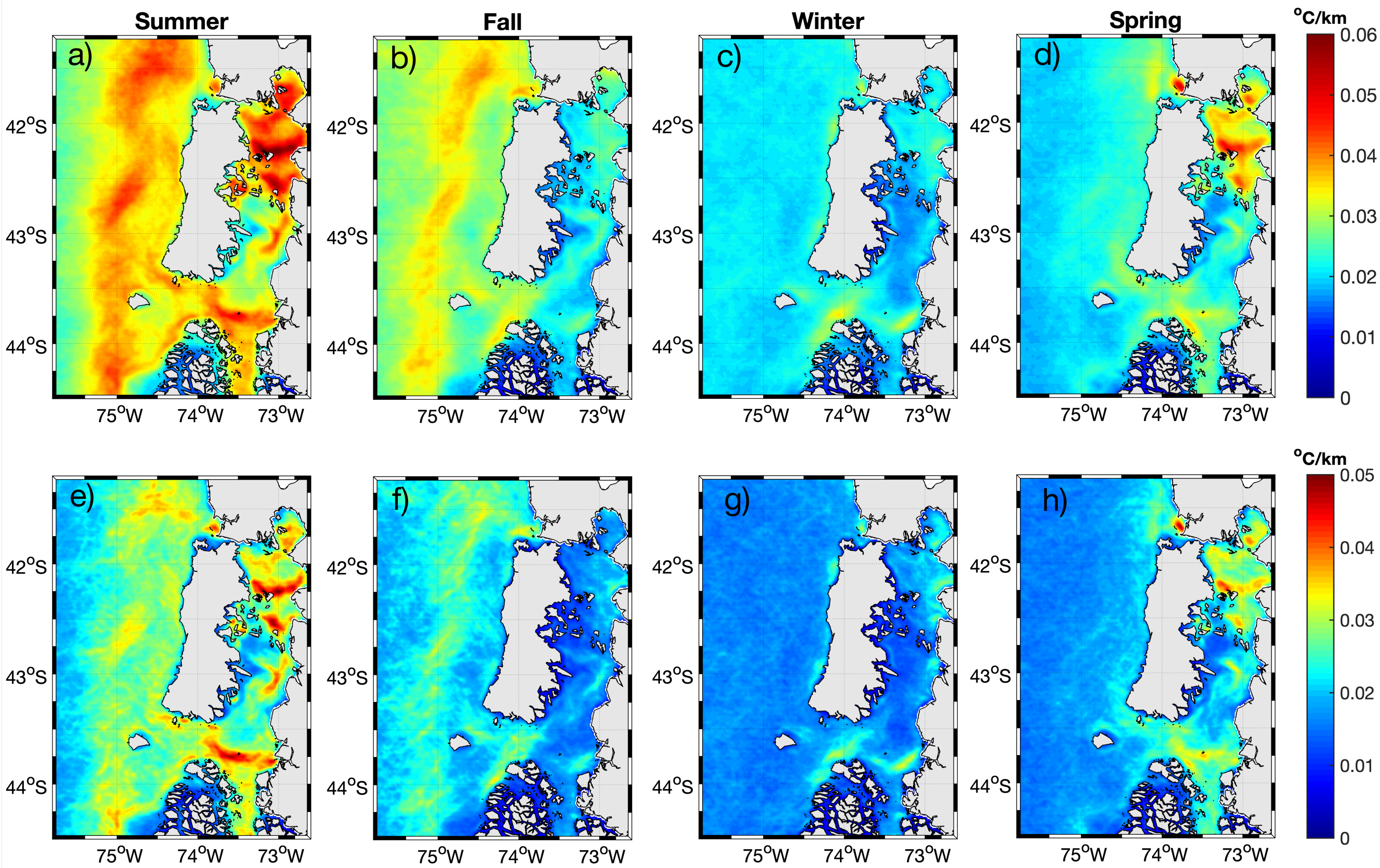

Figure 3. Seasonal climatology (2003–2019) of gradient magnitude of SST in the Inner Sea of Chiloé and its adjacent coastal ocean. (upper panels) averages and (lower panels) standard deviations for (**a**,**e**) summer (January, February, March), (**b**,**f**) fall (April, May, June), (**c**,**g**) winter (July, August, September), and (**d**,**h**) spring (October, November, December). For reference of locations see Figure 1a.

We performed an EOF analysis to separate the main modes of variability of the SST gradient magnitude and evidence the periods when the development of SST fronts in the coastal ocean and the ISC is more likely to occur. The EOFs show that most of the variance is explained in the meridional band of high SST gradients off Chiloé (Figure 5a). These features, highly associated with the upwelling front [22,32], occurred most of the years during December-April (Figure 5c,d). The second EOF isolates the enhanced SST frontal activity in the ISC (Figure 5b), predominantly in spring and early summer (October–February; Figure 5c,d). The temporal oscillations of the EOFs reveal a persistent annual cycle, especially after the end of 2005 (Figure 5d). A maximum SST gradient magnitude in the coastal ocean occurred in early 2008 as seen through the peak of mode 1 (Figure 5d). In northern Patagonia, large-scale climatic influence has been suggested to produce changes in the coastal oceanography, and concomitantly, in ecological patterns around the Inner Sea of Chiloé [21,34]. Future studies focused on the interannual variability of SST fronts should consider the potential impact of climate variability e.g., [21] on the generation or blocking of SST fronts in the ISC.

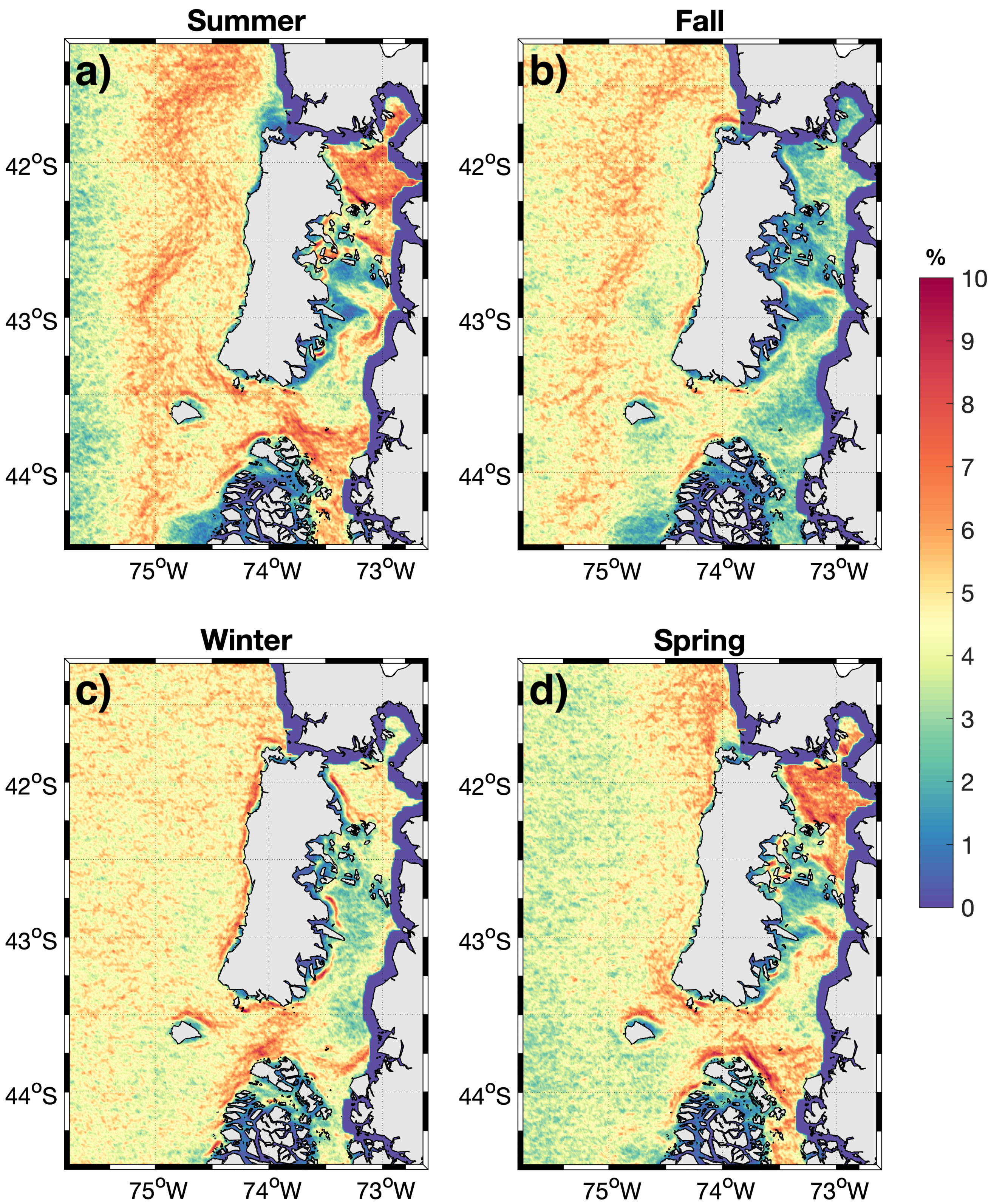

Figure 4. Seasonal climatology (2003–2019) of SST frontal probability (FP; %), based on the Canny edge-detection algorithm, in the Inner Sea of Chiloé and its adjacent coastal ocean for (**a**) summer (January, February, March), (**b**) fall (April, May, June), (**c**) winter (July, August, September), and (**d**) spring (October, November, December). For reference of locations see Figure 1a.

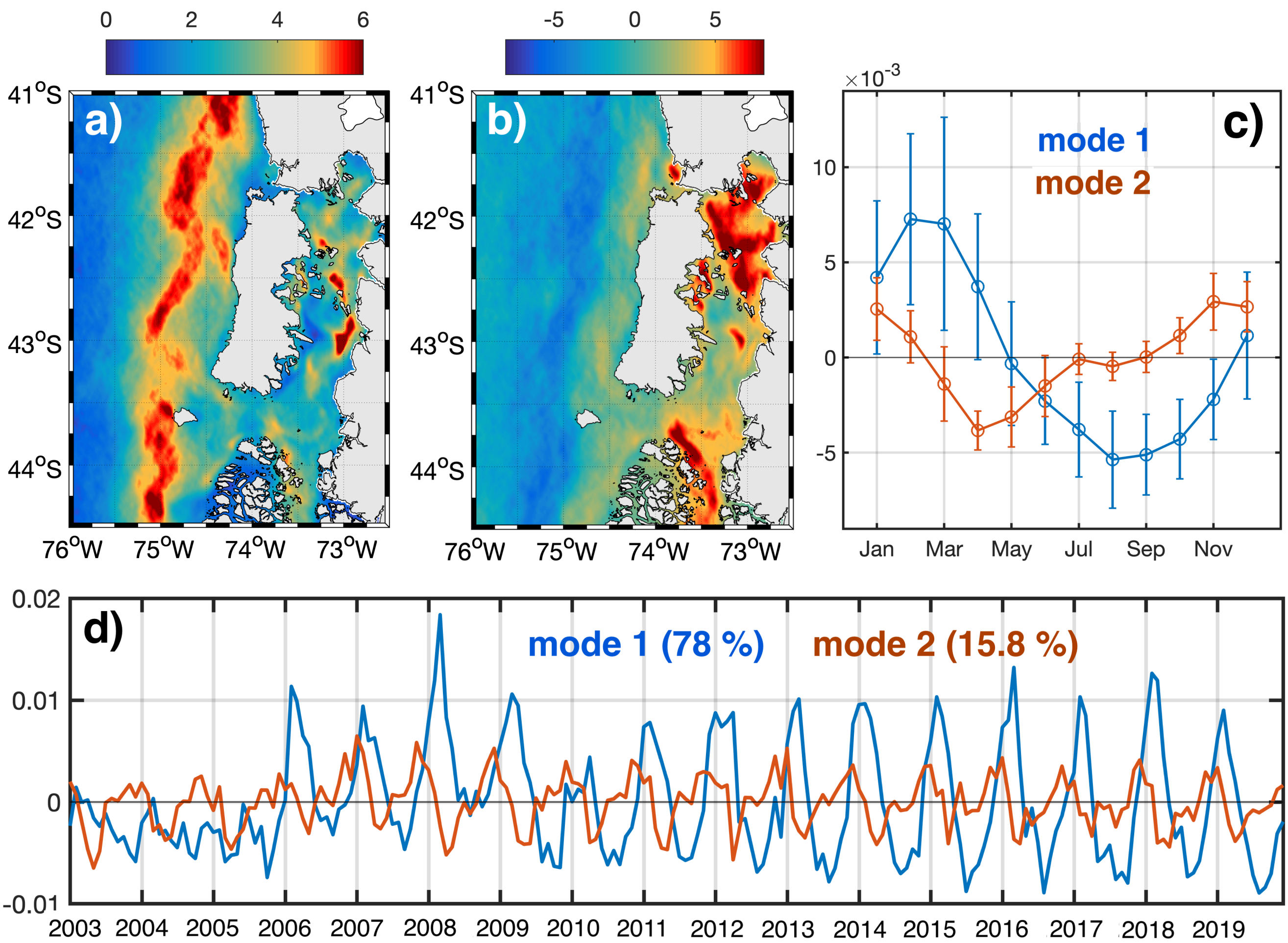

Figure 5. EOF analysis of SST gradient magnitudes. (**a**) First and (**b**) second EOF modes. (**c**) Mean annual cycle of EOF time series shown in (**d**). The error bars in (**c**) correspond to the monthly standard deviations.

The use of satellite platforms to monitor oceanographic properties provides important insights into oceanographic fronts' spatial and temporal variability. An important feature of the northern Patagonian shelf is its significant freshwater inputs [35,36] which could also generate thermal variability and fronts. The river discharges in the northern ISC have been associated with phytoplankton blooms [37]. Freshwater discharge from large rivers and or glacial melting into the Inner Sea of Chiloé (41–45°S) creates a freshwater plume with high levels of biological activity which extends into the coastal ocean [32,38]. While the local impacts of those freshwater discharges remain unknown, it is expected that they would favor the formation of oceanographic fronts and the aggregation of large organisms, such as whales, in the region [39]. Ocean fronts are hotspots of high biological activity [19,40–42] by which increased primary productivity is expected during spring-summer-fall and linked to the areas of high frontal activity (i.e., northern ISC, coastal band off Chiloé Island, southern border of Boca del Guafo). The seasonal climatology of chlorophyll fluorescence (Figure 6) suggests there is enhanced phytoplankton activity around the SST fronts in northern ISC and a maximum fluorescence in a meridional band off Chiloé in fall (Figure 6b), which would agree with the presence of a coastal upwelling frontal band in the coastal ocean (Figure 3b). Thus, northern Patagonia is a highly dynamic region where biophysical interactions over coastal waters remain largely unstudied. The use of satellite products across multiple spatial and temporal scales provides fundamental insights into the oceanographic processes around coastal fronts [43]. Future studies assessing the variability of coastal chlorophyll and productivity in northern Patagonia should focus on regions with enhanced frontal activity to further understand the biophysical coupling at ocean fronts.

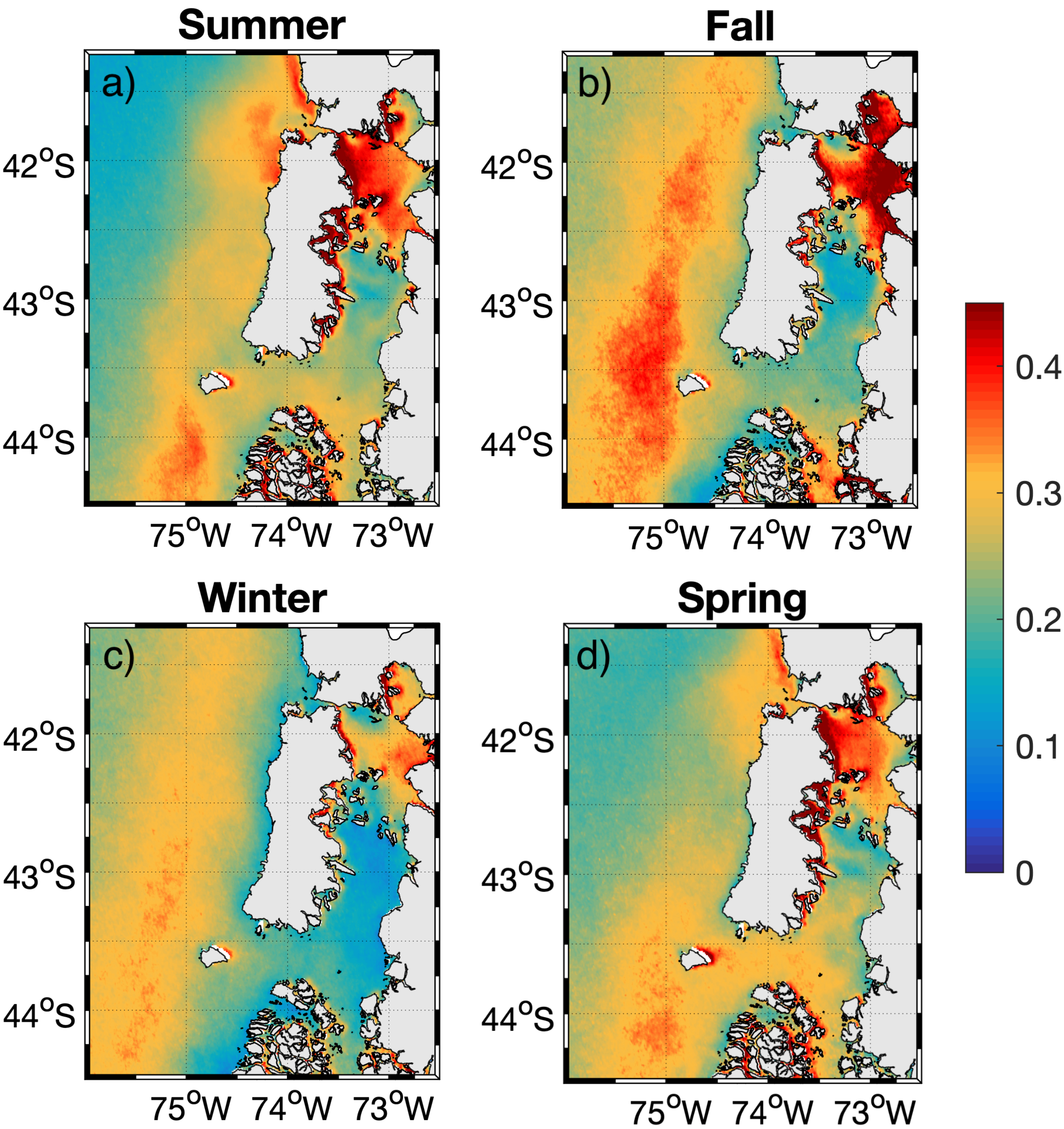

Figure 6. Seasonal climatology (2003–2019) of chlorophyll fluorescence (nFLH; W m^{-2} μm^{-1} sr^{-1}) in the Inner Sea of Chiloé and its adjacent coastal ocean for (**a**) summer (January, February, March), (**b**) fall (April, May, June), (**c**) winter (July, August, September), and (**d**) spring (October, November, December). For reference of locations see Figure 1a.

Potential mechanisms leading to the generation of these fronts could also be related to the bathymetry along the ISC. The northern basin (north of Desertores Islands) has average depths around 300–400 m, whereas the southern ISC is considerably shallower (Figure 1a) [44]. The presence of Desertores Islands limits the water exchange and the circulation between these two sub-regions with distinct regimes of environmental variability [21], which would explain the sharp contrast in SST and frontal activity between these areas (e.g., Figures 2 and 3). The dynamics at Boca del Guafo is likely a major factor influencing the intrusion of oceanic waters and generation of fronts in the southern ISC. Future studies, including field measurements, should focus on sampling the locations with high FP (Figure 4) to understand better the vertical structure and variability of fronts in northern Patagonia.

4. Summary

This study presents the first analyses of SST frontal variability in the Inner Sea of Chiloé and its adjacent coastal ocean. A high correlation with an *in situ* time series in Seno Reloncaví, a region with enhanced frontal variability and high seasonal fluctuations, validates the use of MUR SST fields. The annual cycle of SST gradient magnitudes suggested enhanced frontal activity in northern ISC (north of Desertores Islands) in spring-summer, whereas the coastal ocean off Chiloé presented the highest average gradients in summer and fall. These seasonal patterns are, in general, confirmed by the quantification of the SST frontal probability. Maximum probabilities reached about 10% in northern ISC and off Chiloé. Overall, the southern ISC presented low SST gradient magnitudes and frontal probability yearlong, except for the southern side of Boca del Guafo. An EOF analysis clarified the dominant modes of variability of SST gradient magnitude, highlighting (i) a coastal band of enhanced SST gradients off Chiloé in summer-fall which is coherent with coastal upwelling events and fronts, and (ii) maximum SST fronts in northern ISC and around the southern side of Boca del Guafo in spring-summer. A preliminary inspection of the annual cycle of chlorophyll fluorescence suggests an increased physical-biological coupling around ocean fronts since the highest fluorescence is found in northern ISC and off Chiloé Island, where SST gradient magnitudes and frontal probabilities are maximum. Future studies are suggested to occur in the regions with high frontal activity and considering high-frequency field observations in the surface mixed layer to understand further the dynamics of ocean fronts and their biological implications in northern Patagonia.

Author Contributions: Conceptualization: G.S.S. and W.H.; Methodology: G.S.S., W.H., R.M., C.R.; Investigation: G.S.S., W.H. and L.S.-M.; Resources: G.S.S., C.L. and I.P.-S.; Data curation: G.S.S., S.V., I.P.-S. and L.S.-M.; Writing—original draft preparation: G.S.S. with contribution from all coauthors. All authors have read and agreed to the published version of the manuscript.

Funding: This research was funded by FONDECYT grant number 11190209 and 1190805. GSS was partially funded by the Millennium Nucleus Center for the Study of Multiple Drivers on Marine Socio-Ecological Systems (MUSELS) funded by MINECON NC120028. WH has been funded by MUSELS and Universidad del Bío-Bío. CL has been funded by MUSELS and UPWELL Millenium Nucleus (grant ICM NCN 19153). RM has been funded by Universidad del Bío-Bío. The oceanographic buoy at Seno Reloncaví was funded by FONDEQUIP Grant EQM160167.

Data Availability Statement: MUR data are available at https://podaac.jpl.nasa.gov/dataset/MUR-JPL-L4-GLOB-v4.1). Buoy data at Seno Reloncaví are available at http://www.cdom.cl/estaciones.php?estacion=RLCV&seccion=Oceano. Chlorophyll fluorescence data are available at NASA's ocean color website http://oceancolor.gsfc.nasa.gov.

Conflicts of Interest: The authors declare no conflict of interest. The funders had no role in the design of the study; in the collection, analyses, or interpretation of data; in the writing of the manuscript, or in the decision to publish the results.

References

1. Franks, P.J. Sink or swim: Accumulation of biomass at fronts. *Mar. Ecol. Prog. Ser.* **1992**, *82*, 1–12. [CrossRef]
2. Reese, D.C.; O'Malley, R.T.; Brodeur, R.D.; Churnside, J.H. Epipelagic fish distributions in relation to thermal fronts in a coastal upwelling system using high-resolution remote-sensing techniques. *ICES J. Mar. Sci.* **2011**, *68*, 1865–1874. [CrossRef]
3. Danell-Jiménez, A.; Sanchez-Velasco, L.; Lavín, M.; Marinone, S. Three-dimensional distribution of larval fish assemblages across a surface thermal/chlorophyll front in a semienclosed sea. *Estuar. Coast. Shelf Sci.* **2009**, *85*, 487–496. [CrossRef]
4. Mahadevan, A. Modeling vertical motion at ocean fronts: Are nonhydrostatic effects relevant at submesoscales? *Ocean Model.* **2006**, *14*, 222–240. [CrossRef]
5. Thomas, L.N.; Tandon, A.; Mahadevan, A. Submesoscale processes and dynamics. *Ocean. Model. Eddying Regime* **2008**, *177*, 17–38.
6. Castelao, R.M.; Barth, J.A.; Mavor, T.P. Flow-topography interactions in the northern California Current System observed from geostationary satellite data. *Geophys. Res. Lett.* **2005**, *32*, L24612. [CrossRef]

7. Saldías, G.S.; Allen, S.E. The Influence of a Submarine Canyon on the Circulation and Cross-Shore Exchanges around an Upwelling Front. *J. Phys. Oceanogr.* **2020**, *50*, 1677–1698. [CrossRef]
8. Strub, P.T.; Kosro, P.M.; Huyer, A. The nature of the cold filaments in the California Current System. *J. Geophys. Res.* **1991**, *96*, 14743–14768. [CrossRef]
9. Nieto, K.; Demarcq, H.; McClatchie, S. Mesoscale frontal structures in the Canary Upwelling System: New front and filament detection algorithms applied to spatial and temporal patterns. *Remote Sens. Environ.* **2012**, *123*, 339–346. [CrossRef]
10. Otero, P.; Ruiz-Villarreal, M.; Peliz, A. River plume fronts off NW Iberia from satellite observations and model data. *ICES J. Mar. Sci.* **2009**, *66*, 1853–1864. [CrossRef]
11. Saldías, G.S.; Lara, C. Satellite-derived sea surface temperature fronts in a river-influenced coastal upwelling area off central-southern Chile. *Reg. Stud. Mar. Sci.* **2020**, *37*, 101322. [CrossRef]
12. Ullman, D.S.; Cornillon, P.C. Satellite-derived sea surface temperature fronts on the continental shelf off the northeast US coast. *J. Geophys. Res.* **1999**, *104*, 23459–23478. [CrossRef]
13. Belkin, I. New challenge: Ocean fronts. *J. Mar. Syst.* **2002**, *1*, 1–2. [CrossRef]
14. Belkin, I.M.; Cornillon, P.C.; Sherman, K. Fronts in large marine ecosystems. *Prog. Oceanogr.* **2009**, *81*, 223–236. [CrossRef]
15. Castelao, R.M.; Wang, Y. Wind-driven variability in sea surface temperature front distribution in the California Current System. *J. Geophys. Res.* **2014**, *119*, 1861–1875. [CrossRef]
16. Vazquez-Cuervo, J.; Torres, H.S.; Menemenlis, D.; Chin, T.; Armstrong, E.M. Relationship between SST gradients and upwelling off Peru and Chile: Model/satellite data analysis. *Int. J. Remote Sens.* **2017**, *38*, 6599–6622. [CrossRef]
17. Castelao, R.M.; Mavor, T.P.; Barth, J.A.; Breaker, L.C. Sea surface temperature fronts in the California Current System from geostationary satellite observations. *J. Geophys. Res.* **2006**, *111*. [CrossRef]
18. Vazquez-Cuervo, J.; Dewitte, B.; Chin, T.M.; Armstrong, E.M.; Purca, S.; Alburqueque, E. An analysis of SST gradients off the Peruvian Coast: The impact of going to higher resolution. *Remote Sens. Environ.* **2013**, *131*, 76–84. [CrossRef]
19. Wang, Y.; Castelao, R.M.; Yuan, Y. Seasonal variability of alongshore winds and sea surface temperature fronts in Eastern Boundary Current Systems. *J. Geophys. Res.* **2015**, *120*, 2385–2400. [CrossRef]
20. Wang, Y.; Yu, Y.; Zhang, Y.; Zhang, H.R.; Chai, F. Distribution and variability of sea surface temperature fronts in the south China sea. *Estuar. Coast. Shelf Sci.* **2020**, *240*, 106793. [CrossRef]
21. Lara, C.; Saldías, G.S.; Tapia, F.J.; Iriarte, J.L.; Broitman, B.R. Interannual variability in temporal patterns of Chlorophyll–a and their potential influence on the supply of mussel larvae to inner waters in northern Patagonia (41–44 S). *J. Mar. Syst.* **2016**, *155*, 11–18. [CrossRef]
22. Narváez, D.A.; Vargas, C.A.; Cuevas, L.A.; García-Loyola, S.A.; Lara, C.; Segura, C.; Tapia, F.J.; Broitman, B.R. Dominant scales of subtidal variability in coastal hydrography of the Northern Chilean Patagonia. *J. Mar. Syst.* **2019**, *193*, 59–73. [CrossRef]
23. Iriarte, J.; González, H.; Liu, K.; Rivas, C.; Valenzuela, C. Spatial and temporal variability of chlorophyll and primary productivity in surface waters of southern Chile (41.5–43 S). *Estuar. Coast. Shelf Sci.* **2007**, *74*, 471–480. [CrossRef]
24. León-Muñoz, J.; Urbina, M.A.; Garreaud, R.; Iriarte, J.L. Hydroclimatic conditions trigger record harmful algal bloom in western Patagonia (summer 2016). *Sci. Rep.* **2018**, *8*, 1–10. [CrossRef] [PubMed]
25. Lara, C.; Miranda, M.; Montecino, V.; Iriarte, J.L. Chlorophyll-a MODIS mesoscale variability in the Inner Sea of Chiloé, Patagonia, Chile (41–43° S): Patches and gradients? *Rev. Biol. Mar. Oceanogr.* **2010**, *45*, 217–225. [CrossRef]
26. Canny, J. A computational approach to edge detection. *IEEE Trans. Pattern Anal.* **1986**, *8*, 679–698. [CrossRef]
27. Lara, C.; Saldías, G.S.; Westberry, T.K.; Behrenfeld, M.J.; Broitman, B.R. First assessment of MODIS satellite ocean color products (OC3 and nFLH) in the Inner Sea of Chiloé, northern Patagonia. *Latin Am. J. Aquat. Res.* **2017**, *45*, 822–827. [CrossRef]
28. Emery, W.J.; Thomson, R.E. *Data Analysis Methods in Physical Oceanography*, 2nd ed.; Elsevier: Amsterdam, The Netherlands, 2004.
29. Silva, N.; Calvete, C.; Sievers, H. Masas de agua y circulación general para algunos canales australes entre Puerto Montt y Laguna San Rafael, Chile (Crucero Cimar-Fiordo 1). *Cien. Tecnol. Mar.* **1998**, *21*, 17–48.
30. Acha, E.M.; Mianzan, H.W.; Guerrero, R.A.; Favero, M.; Bava, J. Marine fronts at the continental shelves of austral South America: physical and ecological processes. *J. Mar. Syst.* **2004**, *44*, 83–105. [CrossRef]
31. Tello, A.; Rodriguez-Benito, C. Characterization of mesoscale spatio-temporal patterns and variability of remotely sensed Chl a and SST in the Interior Sea of Chiloe (41.4–43.5°S). *Int. J. Remote Sens.* **2009**, *30*, 1521–1536.
32. Strub, P.T.; James, C.; Montecino, V.; Rutllant, J.A.; Blanco, J.L. Ocean circulation along the southern Chile transition region (38°–46°S): Mean, seasonal and interannual variability, with a focus on 2014–2016. *Prog. Oceanogr.* **2019**, *172*, 159–198. [CrossRef] [PubMed]
33. Pérez-Santos, I.; Seguel, R.; Schneider, W.; Linford, P.; Donoso, D.; Navarro, E.; Amaya-Cárcamo, C.; Pinilla, E.; Daneri, G. Synoptic-scale variability of surface winds and ocean response to atmospheric forcing in the eastern austral Pacific Ocean. *Ocean Sci.* **2019**, *15*, 1247–1266. [CrossRef]
34. Giesecke, R.; Clement, A.; Garcés-Vargas, J.; Mardones, J.I.; González, H.E.; Caputo, L.; Castro, L. Proliferaciones masivas de salpas en el mar interior de la isla de Chiloé (sur de Chile): Posibles causas y consecuencias ecológicas. *Lat. Am. J. Aquat. Res.* **2014**, *42*, 604–621. [CrossRef]
35. Dávila, P.M.; Figueroa, D.; Müller, E. Freshwater input into the coastal ocean and its relation with the salinity distribution off austral Chile (35–55 S). *Cont. Shelf Res.* **2002**, *22*, 521–534. [CrossRef]

36. Calvete, C.; Sobarzo, M. Quantification of the surface brackish water layer and frontal zones in southern Chilean fjords between Boca del Guafo (43 30′ S) and Estero Elefantes (46 30′ S). *Cont. Shelf Res.* **2011**, *31*, 162–171. [CrossRef]
37. Iriarte, J.; León-Muñoz, J.; Marcé, R.; Clément, A.; Lara, C. Influence of seasonal freshwater streamflow regimes on phytoplankton blooms in a Patagonian fjord. *N. Z. J. Mar. Freshw. Res.* **2017**, *51*, 304–315. [CrossRef]
38. Saldías, G.S.; Sobarzo, M.; Quiñones, R. Freshwater structure and its seasonal variability off western Patagonia. *Prog. Oceanogr.* **2019**, *174*, 143–153. [CrossRef]
39. Buchan, S.J.; Quiñones, R.A. First insights into the oceanographic characteristics of a blue whale feeding ground in northern Patagonia, Chile. *Mar. Ecol. Prog. Ser.* **2016**, *554*, 183–199. [CrossRef]
40. Bost, C.A.; Cotté, C.; Bailleul, F.; Cherel, Y.; Charrassin, J.B.; Guinet, C.; Ainley, D.G.; Weimerskirch, H. The importance of oceanographic fronts to marine birds and mammals of the southern oceans. *J. Mar. Syst.* **2009**, *78*, 363–376. [CrossRef]
41. Taylor, J.R.; Ferrari, R. Ocean fronts trigger high latitude phytoplankton blooms. *Geophys. Res. Lett.* **2011**, *38*. [CrossRef]
42. Nieto, K.; Xu, Y.; Teo, S.L.; McClatchie, S.; Holmes, J. How important are coastal fronts to albacore tuna (Thunnus alalunga) habitat in the Northeast Pacific Ocean? *Prog. Oceanogr.* **2017**, *150*, 62–71. [CrossRef]
43. Belkin, I.M.; Cornillon, P.C. Fronts in the world ocean's large marine ecosystems. *ICES CM* **2007**, *500*, 21.
44. González, H.; Calderón, M.; Castro, L.; Clement, A.; Cuevas, L.; Daneri, G.; Iriarte, J.; Lizárraga, L.; Martínez, R.; Menschel, E.; et al. Primary production and plankton dynamics in the Reloncaví Fjord and the Interior Sea of Chiloé, Northern Patagonia, Chile. *Mar. Ecol. Prog. Ser.* **2010**, *402*, 13–30. [CrossRef]